



HAL
open science

On the Consistency of the Conventional Gait Model Across Various Pose Estimation Algorithms

Fabien Leboeuf, Stephane Armand, Mickael Fonseca, Henrike Greaves, July
Reay, Morgan Sangeux

► **To cite this version:**

Fabien Leboeuf, Stephane Armand, Mickael Fonseca, Henrike Greaves, July Reay, et al.. On the Consistency of the Conventional Gait Model Across Various Pose Estimation Algorithms. 2024. hal-04665267

HAL Id: hal-04665267

<https://hal.science/hal-04665267v1>

Preprint submitted on 2 Aug 2024

HAL is a multi-disciplinary open access archive for the deposit and dissemination of scientific research documents, whether they are published or not. The documents may come from teaching and research institutions in France or abroad, or from public or private research centers.

L'archive ouverte pluridisciplinaire **HAL**, est destinée au dépôt et à la diffusion de documents scientifiques de niveau recherche, publiés ou non, émanant des établissements d'enseignement et de recherche français ou étrangers, des laboratoires publics ou privés.



Distributed under a Creative Commons Attribution 4.0 International License

Cliquez ou appuyez ici pour entrer du texte.

On the Consistency of the Conventional Gait Model Across Various Pose Estimation Algorithms

Leboeuf F. ^{1,2}, Armand S. ³, Fonseca, M³, Greaves H. ^{4,5}, Reay J. ², Sangeux M. ⁶

1 Motion analysis service, Physical Medicine and Rehabilitation, Teaching Hospital of Nantes, France

2 School of Health & Society, The University of Salford, UK

3 Kinesiology Laboratory, Geneva University Hospitals and University of Geneva, Geneva, Switzerland

4 North West Motion Analysis Centre, Alder Hey Children's NHS Foundation Trust, UK

5 Research Institute for Sport and Exercise Sciences, Liverpool John Moores University, UK

5 University Children's Hospital Basel, Switzerland

Acknowledgments:

This work was supported by The University of Salford, United-Kingdom. Funding was also provided by Vicon (Oxford, UK) and Qualisys (Goteborg, Sweden).

Corresponding author:

Fabien Leboeuf

Motion Analysis Service, Physical Medicine and Rehabilitation

Teaching hospital of Nantes

85 rue Saint Jacques

44093 Nantes, FRANCE

email: fabien.leboeuf@chu-nantes.com

Abstract word count: 229 words

Document word count: 2348 words

ABSTRACT

Background:

Clinical gait analysis uses the Conventional Gait Model (CGM) to assess neuromusculoskeletal deficiencies in walking. While various software supports CGM processing, limitations exist in current pose estimation algorithms, such as their inability to maintain consistent segment lengths or joint translations, adequate for musculoskeletal modelling.

Research question:

This study investigates the impact of different pose estimation algorithms on the kinematics generated from the conventional gait model and aims to verify the assumption that different algorithms produce comparable results.

Methods:

The study involved 36 participants, including 24 healthy individuals and 12 individuals with cerebral palsy. Using the pyCGM2 library, various CGM-compatible pose estimation algorithms, including a non-optimizing native method (NONOPT), a 6 degrees of freedom method, and kinematic fitting approaches, were implemented. Algorithms were evaluated using the mean absolute deviation (MAD) and adjusted r-squared metrics to compare angle outputs.

Results:

The study found minimal differences (under 5°) in lower limb angles between the pose estimation methods. The inclusion of additional skin markers and the application of a Kalman filter-based method showed only slight increases in MAD, suggesting robustness across methods, especially in sagittal plane kinematics.

Significance:

This study confirms the utility of advanced computational methods in clinical gait analysis, supporting the integration of musculoskeletal modeling in clinical settings. The findings facilitate the continued use of the CGM, ensuring that computational advances do not compromise the interpretability of gait analysis outcomes.

KEYWORDS: Gait analysis, conventional gait model, segmental pose, segmental optimisation, inverse kinematics.

1 INTRODUCTION

Clinical gait analysis (CGA) provides an objective record of the neuromusculoskeletal deficiencies limiting an individual's functional walking ability [1]. CGA follows standards [2] and recommendations [3], and may occur in a variety of settings [4]. Specialised commercial software have been developed to support the processing of clinical biomechanics models [5–7]. However, modifying the data processing protocol by integrating new or modified methods, even those recognised as clinically relevant in the literature [8], is not straightforward. The main difficulty is the lack of backward compatibility which would prevent true comparison between data processed by different models across time.

Most CGA laboratories use the Conventional Gait Model (CGM) [7], which was distributed under the commercial name *Vicon Plugin Gait* (Vicon, Oxford Metrics, Oxford UK) for a long time [4]. This model is characterized by i) a small number of markers placed only on the lateral parts of the lower limbs, of which two markers are mounted on wands, and ii) a method of estimating segment poses that does not involve optimisation, since the body coordinate systems are constructed frame-by-frame from the measured marker trajectories [5,7,9]. Replications of the CGM model outside Vicon commercial software are possible with Python [10]. The CGM-like model by C-motion Inc (C-motion, Inc., Germantown MD, USA) [11], replicates the anatomical definitions but employs a different segment pose algorithm based on least squares optimisation [9], also called 6 degrees of freedom (6DoF), assuming this pose estimator produces results substantially similar to the native CGM. To the best of our knowledge, this assumption has never been verified. Some users of this CGM-like model [12] mentioned their findings may not be extrapolated to the native CGM.

Both frame-by-frame and 6DoF pose estimation algorithms may provide inadequate results for use with musculoskeletal modelling because these pose estimation algorithms do not guarantee either constant segment lengths or pre-defined joint translations in the presence of soft tissue artefact (STA) [13]. However, musculoskeletal modelling may be required to estimate clinically relevant information about muscle function during gait ([14,15]). Pose estimation algorithms for musculoskeletal modelling require kinematic fitting of the entire articulated, multibody, model with a predefined number of DoF at each joint [16–18]. This approach may be called inverse kinematics, multibody, or global optimisation [19] and is implemented in multiple musculoskeletal modelling software [18,20].

Kinematic fitting (KF) is known to be sensitive to joint constraints [12,17,18] and markersets [10]. Kainz et al. [16] showed that, compared to the anatomical definitions of joint centres and segment axes, pose estimation algorithms may not be the primary source of differences between models.

This study aimed to isolate the effect of different pose estimation algorithms, including KF, on the outputs of the CGM, by testing these algorithms across different markersets. The open-source pyCGM2 library [10] was utilised to implement the different pose estimation algorithms on top of a validated replication of the native CGM. We also aimed to quantify the effects of the KF solver precision and implemented a method based on Kalman filtering [21].

2 Materials and Methods

2.1.1 Participants

Twenty-four healthy participants (mean (sd) age: 19.3 (10.2) years old, height: 1.56 (0.20) m, weight: 51.3 (19.8) kg, and body mass index: 20.2 (4.4) kg.m⁻²) and 12 subjects with cerebral palsy (CP) (age: 18.2 (9.1) years old, height: 1.57 (0.16) m, weight: 50.1 (18.2) kg, and body mass index: 20.1 (4.3) kg.m⁻²) were recruited. Informed consent was obtained, and the protocol conformed to the Declaration of Helsinki and was approved by the Institutional Review Board (“Commission Cantonale d’Éthique de la Recherche de Genève” (CCER-2020-00358)).

2.1.2 Data collection

The 3D trajectories of 23 skin-mounted and 4 wand-mounted light-reflective markers were recorded using a 12-camera optoelectronic system (Oqus7+, Qualisys, Sweden) sampled at 100 Hz. Figure 1 and Table 1 detail the location of the markers. Markers were placed according to the CGM markerset CGM2.3 [10,22]. All measurements were undertaken by a physiotherapist with several years’ experience of conducting 3DGA.

Marker trajectories were filtered with Butterworth fourth order with a cutting frequency of 6 Hz.

2.1.3 Model processing

Knee and ankle joint centres were calibrated as the mid-point between the lateral and medial epicondyles or malleoli markers, respectively. The hip joint centres were calculated from the pelvis pose, using the predictive equations of Hara [23]. No correction of the knee varus-valgus was applied. These definitions were the same for all pose estimation algorithms.

We considered the following pose estimation methods:

- The *NONOPT* algorithm is the native method of the CGM [10]. Thigh (or shank) rotation angle offset is calculated to align the coronal plane with the plane formed by the proximal joint centre, the distal joint centre, and the epicondyle (or malleolus) markers during static calibration. The coronal plane is formed from the frame-by-frame lateral wand / lateral epicondyle (or malleolus) and proximal joint centre marker trajectories first and then rotated by the static offset. This model is versioned as CGM2.1 in the pyCGM2 library [24].
- The *6DOF-CGM* method tracks the thigh (resp. shank) segment from the singular decomposition [25] of a cluster made of the (virtual) hip joint centre, the lateral thigh wand marker (THI) and the lateral knee condyles (KNE) (resp. the knee joint centre, the lateral shank wand marker (TIB) and the lateral malleolus (ANK)).
- The *KF* algorithm considers a multibody model with all joints limited to three rotational degrees of freedom. All tracking markers (Table 1) participated to the optimisation process. The same weight was assigned to all markers and KF was performed using

OpenSim API [26]. We set the solver accuracy to 10^{-5} (default OpenSim value) and 10^{-8} , and performed KF for two markersets:

- *KF-CGM2.2*, i.e., the native CGM markerset.
- *KF-CGM2.3*, i.e., the CGM markerset supplemented with two additional markers located on the thigh and shank segments, used as tracking markers.

The use of KF instead of NONOPT is versioned as CGM2.2 in pyCGM2. The version CGM2.3 refers to the use KF with skin markers (no wands).

- The Kalman-smoother KF algorithm (*KKF*) includes prior knowledge about the smoothness of the motion [21]. The process makes the state of the model not independent between two frames. We interfaced *KKF* software distributed online (<https://simtk.org/projects/kalmanforik>) with pyCGM2. The same weight was assigned to all markers. The solver accuracy and the estimate of the standard deviation of the measured marker were set to the default values. We performed *KKF* for the two markersets:
 - *KKF-CGM2.2*, i.e., the native CGM markerset.
 - *KKF-CGM2.3*, i.e., the native CGM markerset supplemented with two additional markers located on the thigh and shank segments, used as tracking markers (see figure 1).

All kinematic fitting methods were preceded by a scaling of the gait2392 model provided by OpenSim. This scaling utilised inter-joint centres distances so that the scaled model adheres to the localisation of the joint centres of the native CGM.

2.1.4 Data processing

All computations were performed with the open-source package pyCGM2 [10]. Gait events were detected using force plate foot contacts, and visually checked. For healthy participants, we gathered the dominant and non-dominant lower limbs. For the pathological subjects, we only focused on the impaired limb. We analysed 1131 and 487 cycles for healthy and CP subjects respectively.

Overall comparisons of angles from each tracking method were evaluated through the Mean Absolute Deviation (MAD) calculated as follows from a gait cycle:

$$MAD = \left(\frac{1}{n} \sum_{i=0}^{n-1} |q_i(\text{Method}_1) - q_i(\text{Method}_2)| \right) \quad (1)$$

where i is the gait cycle timing, ranging from 1 to n , q stands for angles and methods 1 and 2 represent two distinct segmental tracking methods.

Curve similarity was quantified with the adjusted r^2 [26]. Interpretation of the coefficient followed rules [26]: Strong correlation ($r^2 > 0.9$); high ($0.7 < r^2 \leq 0.9$); moderate ($0.5 \leq r^2 < 0.7$), low ($0.3 \leq r^2 < 0.5$), negligible ($r^2 < 0.3$)

2.1.5 Comparisons

Our study focused on three comparisons, as illustrated in Table 2. The first comparison aimed to evaluate the difference between each of the tracking methods and the native method of the CGM, i.e., the NONOPT method. The second comparison (*within-marker set – between KF methods*) compared the KF methods one by one for the same marker set, either the native marker set or the augmented marker set. The last comparison (*between-marker sets – within KF method*) examined the kinematics produced by the two marker sets for the same KF method.

3 Results

The different pose estimation algorithms impacted the transverse plane the most, both for healthy participants and CP subjects. Table 2 summarises the results for the kinematics with the largest differences between models, marker sets, and solver accuracy (KF method only). All results are available in supplementary materials. Transverse plane rotation of the hip was the angle that presented the largest MAD (Table 2). With the marker set of the native CGM, the average MAD ranged between 2.0° and 2.6° . The maximum reached 4.3° degrees with the KKF method. The correlations were high (larger than 0.7) (Table 3).

The addition of skin markers increased the average MAD compared with the NONOPT method. The MAD was of 4° for both of our populations and exceeded 5° in one subject with CP. The correlations were predominantly high, except for knee abduction, internal hip rotation, and pelvic obliquity, which presented moderate correlations (ranging from 0.5 to 0.7). Figures 3 and 4 depict the differences in the curves for the two samples. The curves diverged mostly during the second double support and early swing phases.

The *between-marker sets – within KF method* comparisons showed MAD less than 1° , with excellent correlations ($r^2 > 0.7$). However, even if the correlations of the *between-marker sets – within KF method* comparisons remained high, the average MAD ranged between 3.2° and 3.7° , and their maximum reached 6.7° and 7.7° , respectively, for a healthy participant and one subject with CP (Table 2).

4 Discussion

The aim of this study was to investigate the effects of various pose estimation algorithms on lower limb kinematics of walking for the CGM model using different marker sets. We found a small effect of the pose estimation algorithms and marker sets. In healthy participants and subjects with CP, we showed that there were differences of less than 5° between the 6DOF, NONOPT, Kinematic Fitting, and Kalman-smoothing Kinematic Fitting methods.

Comparing our results with the literature is challenging due to the heterogeneity in variables of interest (discrete points, range of motion) and techniques used (skin clusters, rigid clusters, wand-mounted markers). Nonetheless, we observed a similar behaviour in our results to those previously reported, namely i) robust sagittal plane kinematics with mean MAD less than 2.1° , ii) deviations mainly impacting transverse plane rotations, specifically the hip (maximum mean MAD: 4.2°), and iii) shape changes of the knee abduction curve during the transition from the stance to the swing

phases. Our results were consistent with those of Kainz [16], showing an error of less than 5° for all lower limb angles between tracking methods when the model shares the same definition of segmental references and the same number of markers. Similarly, like Mentipley et al. [12] and Mantovani et al. [27], we observed increased differences when new tracking markers were added (CGM 2.3). However, our results disagree with Langley et al. [28], who showed that the 6DOF method resulted in deviations greater than 5° when applied either to a marker placed laterally on the skin or to a rigid cluster of 4 markers. Their placement of the lateral skin marker, more proximal, may have been influenced by increased STA near the joint [29].

Our results shows the CGM may be used with a KF method with limited impact on kinematics. Previously, Hayford et al. [17] demonstrated that while KF altered the Gait Profile Score (GPS) [30], it did not change clinical judgment. However, Hayford [17] did not model all joints with 3DoF, as is the case of the CGM.

In this study, all procedures were conducted using the open-source library pyCGM2 [10], which is also integrated in motion capture software distributed by Vicon or Qualisys. The KF methods used the OpenSim API. These operations are transparent to the user, furthermore a video of the process is available in supplementary data. Importantly, scaling of the musculoskeletal model ensured the appropriate localisation of the joint centres in the presented process. Without such scaling, comparisons would not be grounded in the same anatomical definitions, and differences might exceed 5°, as evidenced in Ziziene et al. [31] who reported a mean difference across all lower limb joints of 13°.

To maintain backward compatibility with the native CGM, KF was implemented using a markerset that included wand-mounted markers. These may be substituted with skin markers. Leboeuf and Sangeux [9] showed that the anteroposterior displacement of the lateral shank marker was less with skin markers. KF may provide results less affected by STA.

There were minimal differences due to the change in precision of the KF solver from $10e^{-5}$ to $10e^{-8}$ or the use of a numerical solver based on Kalman filtering. By default, OpenSim implements a precision of $10e^{-5}$. Although we did not obtain differences for the MAD, we recommend maintaining a precision of $10e^{-8}$. This increases the calculation time (on average by + 10%) but avoids singularity in kinematic curves. Kalman filtering significantly reduced calculation time (on average by -20%). It constitutes a viable solution for long acquisition (e.g., on a treadmill) or real-time estimation of kinematic, dynamic, and muscular data [32].

The study is subject to limitations. Firstly, we do not have a reference for the true orientation of the bones in space. We reported here the difference between tracking methods without knowing their trueness. Secondly, we have only used the KF solver available through OpenSim. Other resources, from other musculoskeletal modelling solutions, may lead to different results. Thirdly, we tested the different algorithms for a sample of GMFCS 1 and 2 CP subjects, further investigations may be undertaken in patients with more severe or other musculoskeletal disorders.

In conclusion, our study has evaluated the different segmental tracking methods currently available in the literature. The differences between the methods are inferior to 5°, and different markersets have a minor influence. Utilising the pyCGM2 calculation library as a resource, current CGM users are afforded the opportunity to advance computational methods and foster the adoption of musculoskeletal modelling. This innovation has the potential to enhance clinical reasoning and provide new insight in clinical gait analysis.

References

- [1] R. Baker, A. Esquenazi, M.G. Benedetti, K. Desloovere, Gait analysis: clinical facts, *European journal of physical and rehabilitation medicine* 52 (2016) 560–574.
- [2] Clinical Movement Analysis Society-UK and Ireland, *Clinical Movement Analysis Standards*, 2023.
- [3] M.G. Benedetti, E. Beghi, A. de Tanti, A. Cappozzo, N. Basaglia, A.G. Cutti, A. Cereatti, R. Stagni, F. Verdini, M. Manca, S. Fantozzi, C. Mazzà, V. Camomilla, I. Campanini, A. Castagna, L. Cavazzuti, M. Del Maestro, U. Della Croce, M. Gasperi, T. Leo, P. Marchi, M. Petrarca, L. Piccinini, M. Rabuffetti, A. Ravaschio, Z. Sawacha, F. Spolaor, L. Tesio, G. Vannozzi, I. Visintin, M. Ferrarin, SIAMOC position paper on gait analysis in clinical practice: General requirements, methods and appropriateness. Results of an Italian consensus conference, *Gait & posture* 58 (2017) 252–260.
<https://doi.org/10.1016/j.gaitpost.2017.08.003>.
- [4] S. Armand, Z. Sawacha, M. Goudriaan, B. Horsak, M. van der Krogt, C. Huenaerts, C. Daly, A. Kranzl, H. Boehm, M. Petrarca, A. Guiotto, A. Merlo, F. Spolaor, I. Campanini, M. Cosma, A. Hallemans, H. Horemans, D. Gasq, F. Moissenet, A. Assi, M. Sangeux, Current practices in clinical gait analysis in Europe: A comprehensive survey-based study from the European society for movement analysis in adults and children (ESMAC) standard initiative, *Gait & posture* 111 (2024) 65–74.
<https://doi.org/10.1016/j.gaitpost.2024.04.014>.
- [5] M.P. Kadaba, H.K. Ramakrishnan, M.E. Wootten, Measurement of lower extremity kinematics during level walking, *Journal of orthopaedic research official publication of the Orthopaedic Research Society* 8 (1990) 383–392.
<https://doi.org/10.1002/jor.1100080310>.
- [6] R.B. Davis, S. Öunpuu, D. Tyburski, J.R. Gage, A gait analysis data collection and reduction technique, *Human movement science* 10 (1991) 575–587.
[https://doi.org/10.1016/0167-9457\(91\)90046-Z](https://doi.org/10.1016/0167-9457(91)90046-Z).
- [7] R. Baker, F. Leboeuf, J. Reay, M. Sangeux, The Conventional Gait Model - Success and Limitations, in: B. Müller, S. Wolf, G.-P. Brueggemann, Z. Deng, F. Miller, W.S. Selbie (Eds.), *Handbook of human motion*, Springer International Publishing, [Switzerland?], 2016, pp. 1–19.

- [8] R. Baker, Pelvic angles: a mathematically rigorous definition which is consistent with a conventional clinical understanding of the terms, *Gait & posture* 13 (2001) 1–6. [https://doi.org/10.1016/s0966-6362\(00\)00083-7](https://doi.org/10.1016/s0966-6362(00)00083-7).
- [9] F. Leboeuf, M. Sangeux, Wand-mounted lateral markers are less prone to soft-tissue artefacts than skin-mounted markers when using the conventional gait model, *Gait & posture* (2022). <https://doi.org/10.1016/j.gaitpost.2022.12.013>.
- [10] F. Leboeuf, R. Baker, A. Barré, J. Reay, R. Jones, M. Sangeux, The conventional gait model, an open-source implementation that reproduces the past but prepares for the future, *Gait & posture* 69 (2019) 235–241. <https://doi.org/10.1016/j.gaitpost.2019.04.015>.
- [11] C-motion, Tutorial: Building a Conventional Gait Model: (<https://www.c-motion.com/v3dwiki/index.php>).
- [12] B.F. Mentiplay, R.A. Clark, Modified conventional gait model versus cluster tracking: Test-retest reliability, agreement and impact of inverse kinematics with joint constraints on kinematic and kinetic data, *Gait & posture* 64 (2018) 75–83. <https://doi.org/10.1016/j.gaitpost.2018.05.033>.
- [13] A. Leardini, L. Chiari, U. Della Croce, A. Cappozzo, Human movement analysis using stereophotogrammetry. Part 3. Soft tissue artifact assessment and compensation, *Gait & posture* 21 (2005) 212–225. <https://doi.org/10.1016/j.gaitpost.2004.05.002>.
- [14] T.A. Correa, K.M. Crossley, H.J. Kim, M.G. Pandy, Contributions of individual muscles to hip joint contact force in normal walking, *Journal of biomechanics* 43 (2010) 1618–1622. <https://doi.org/10.1016/j.jbiomech.2010.02.008>.
- [15] H. Kainz, H. Hoang, L. Pitto, M. Wesseling, S. van Rossom, A. van Campenhout, G. Molenaers, F. de Groote, K. Desloovere, I. Jonkers, Selective dorsal rhizotomy improves muscle forces during walking in children with spastic cerebral palsy, *Clinical biomechanics (Bristol, Avon)* 65 (2019) 26–33. <https://doi.org/10.1016/j.clinbiomech.2019.03.014>.
- [16] H. Kainz, L. Modenese, D.G. Lloyd, S. Maine, H.P.J. Walsh, C.P. Carty, Joint kinematic calculation based on clinical direct kinematic versus inverse kinematic gait models, *Journal of biomechanics* 49 (2016) 1658–1669. <https://doi.org/10.1016/j.jbiomech.2016.03.052>.
- [17] C.F. Hayford, E. Pratt, J.P. Cashman, O.G. Evans, C. Mazzà, Effectiveness of Global Optimisation and Direct Kinematics in Predicting Surgical Outcome in Children with Cerebral Palsy, *Life (Basel, Switzerland)* 11 (2021). <https://doi.org/10.3390/life11121306>.

- [18] A. Seth, J.L. Hicks, T.K. Uchida, A. Habib, C.L. Dembia, J.J. Dunne, C.F. Ong, M.S. DeMers, A. Rajagopal, M. Millard, S.R. Hamner, E.M. Arnold, J.R. Yong, S.K. Lakshmikanth, M.A. Sherman, J.P. Ku, S.L. Delp, OpenSim: Simulating musculoskeletal dynamics and neuromuscular control to study human and animal movement, *PLoS computational biology* 14 (2018) e1006223. <https://doi.org/10.1371/journal.pcbi.1006223>.
- [19] M. Begon, M.S. Andersen, R. Dumas, Multibody Kinematics Optimization for the Estimation of Upper and Lower Limb Human Joint Kinematics: A Systematized Methodological Review, *Journal of biomechanical engineering* 140 (2018). <https://doi.org/10.1115/1.4038741>.
- [20] M. Damsgaard, J. Rasmussen, S.T. Christensen, E. Surma, M. de Zee, Analysis of musculoskeletal systems in the AnyBody Modeling System, *Simulation Modelling Practice and Theory* 14 (2006) 1100–1111. <https://doi.org/10.1016/j.simpat.2006.09.001>.
- [21] F. de Groot, T. de Laet, I. Jonkers, J. de Schutter, Kalman smoothing improves the estimation of joint kinematics and kinetics in marker-based human gait analysis, *Journal of biomechanics* 41 (2008) 3390–3398. <https://doi.org/10.1016/j.jbiomech.2008.09.035>.
- [22] S. van Sint Jan, *Color Atlas of Skeletal Landmark Definitions E-Book: Guidelines for Reproducible Manual and Virtual Palpations*, Churchill Livingstone, St. Louis, 2007.
- [23] R. Hara, J. McGinley, C. Briggs, R. Baker, M. Sangeux, Predicting the location of the hip joint centres, impact of age group and sex, *Scientific reports* 6 (2016) 37707. <https://doi.org/10.1038/srep37707>.
- [24] F. Leboeuf, J. Reay, R. Jones, M. Sangeux, The effect on conventional gait model kinematics and kinetics of hip joint centre equations in adult healthy gait, *Journal of biomechanics* 87 (2019) 167–171. <https://doi.org/10.1016/j.jbiomech.2019.02.010>.
- [25] F.E. Veldpaus, H.J. Woltring, L. Dortmans, A least-squares algorithm for the equiform transformation from spatial marker co-ordinates, *Journal of biomechanics* 21 (1988) 45–54. [https://doi.org/10.1016/0021-9290\(88\)90190-X](https://doi.org/10.1016/0021-9290(88)90190-X).
- [26] M. Iosa, A. Cereatti, A. Merlo, I. Campanini, S. Paolucci, A. Cappozzo, Assessment of waveform similarity in clinical gait data: the linear fit method, *BioMed research international* 2014 (2014) 214156. <https://doi.org/10.1155/2014/214156>.
- [27] G. Mantovani, M. Lamontagne, How Different Marker Sets Affect Joint Angles in Inverse Kinematics Framework, *Journal of biomechanical engineering* 139 (2017). <https://doi.org/10.1115/1.4034708>.

- [28] B. Langley, A. Jones, T. Board, M. Greig, Modified conventional gait model vs. Six degrees of freedom model: A comparison of lower limb kinematics and associated error, *Gait & posture* 89 (2021) 1–6. <https://doi.org/10.1016/j.gaitpost.2021.06.016>.
- [29] A. Cappozzo, Three-dimensional analysis of human walking: Experimental methods and associated artifacts, *Human movement science* 10 (1991) 589–602. [https://doi.org/10.1016/0167-9457\(91\)90047-2](https://doi.org/10.1016/0167-9457(91)90047-2).
- [30] R. Baker, J.L. McGinley, M.H. Schwartz, S. Beynon, A. Rozumalski, H.K. Graham, O. Tirosh, The gait profile score and movement analysis profile, *Gait & posture* 30 (2009) 265–269. <https://doi.org/10.1016/j.gaitpost.2009.05.020>.
- [31] Jurgita Ziziene, Kristina Daunoraviciene, Giedre Juskeniene, Juozas Raistenskis, Comparison of kinematic parameters of children gait obtained by inverse and direct models.
- [32] C. Pizzolato, M. Reggiani, L. Modenese, D.G. Lloyd, Real-time inverse kinematics and inverse dynamics for lower limb applications using OpenSim, *Computer methods in biomechanics and biomedical engineering* 20 (2017) 436–445. <https://doi.org/10.1080/10255842.2016.1240789>.

Captions of figures and tables

Figure 1: Marker set

Figure 2: Kinematic gait panel provided from the different segmental poses. The plotted data is the mean curve for the entire cohort of healthy participants.

Figure 3: Kinematic gait panel provided from the different segmental poses. The plotted data is the mean curve for the entire cohort of CP subjects.

Table 1: Description of the marker locations.

Table 2: The table resumes the 3 undertaken comparisons, i) the comparison of all methods with the NONOPT method, ii) the *within-marker set – between KF methods* comparisons and iii) the *between-marker sets – within KF method* comparisons. For each comparison, we reported [the mean MAD (standard deviation) – maximum MAD] of the most impacted angle.

Table 3: Mean Absolute Deviation (MAD). The subtable a) gathers the comparison of all methods with the NONOPT method, and the the *within-marker sets – between KF methods* comparisons. Subtable b) presents the *between-marker sets – within KF method* comparisons.

Table 4: Correlation (r^2). The subtable a) gathers the comparison of all methods with the NONOPT method, and the the *within-marker sets – between KF methods* comparisons. Subtable b) presents the *between-marker sets – within KF method* comparisons.

Figure 1

Cliquez ou appuyez ici pour entrer du texte.

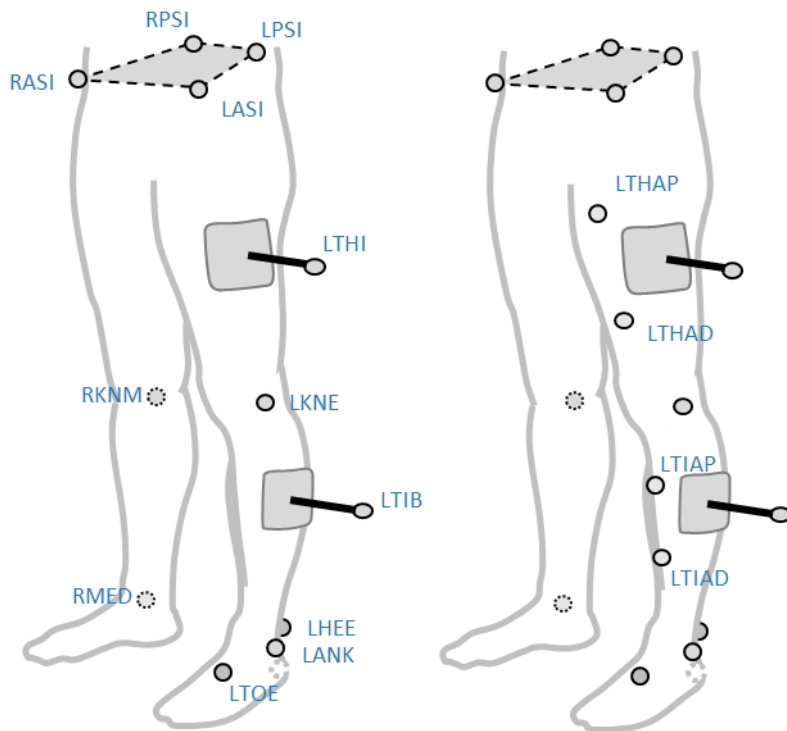


Figure 2

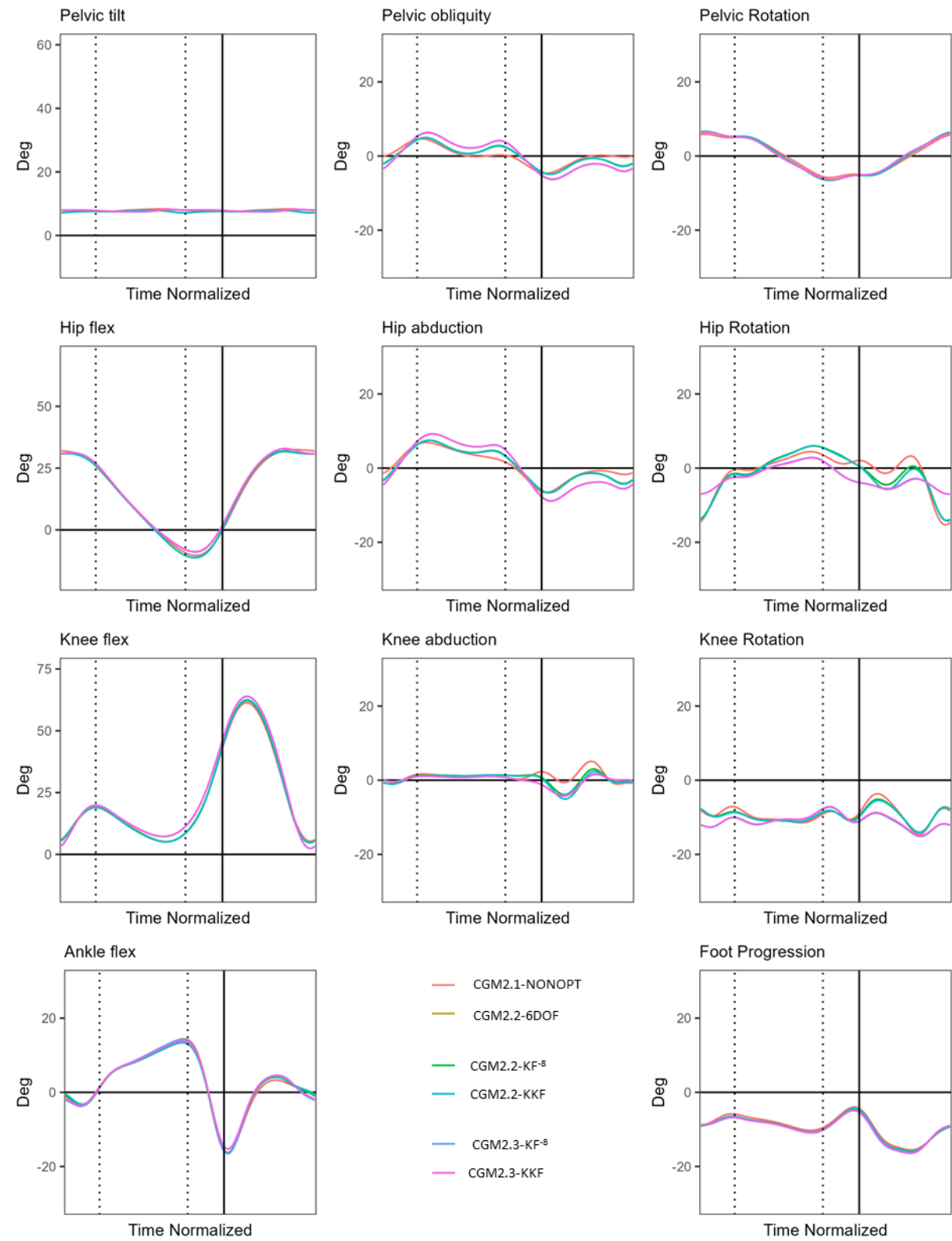


Figure 3

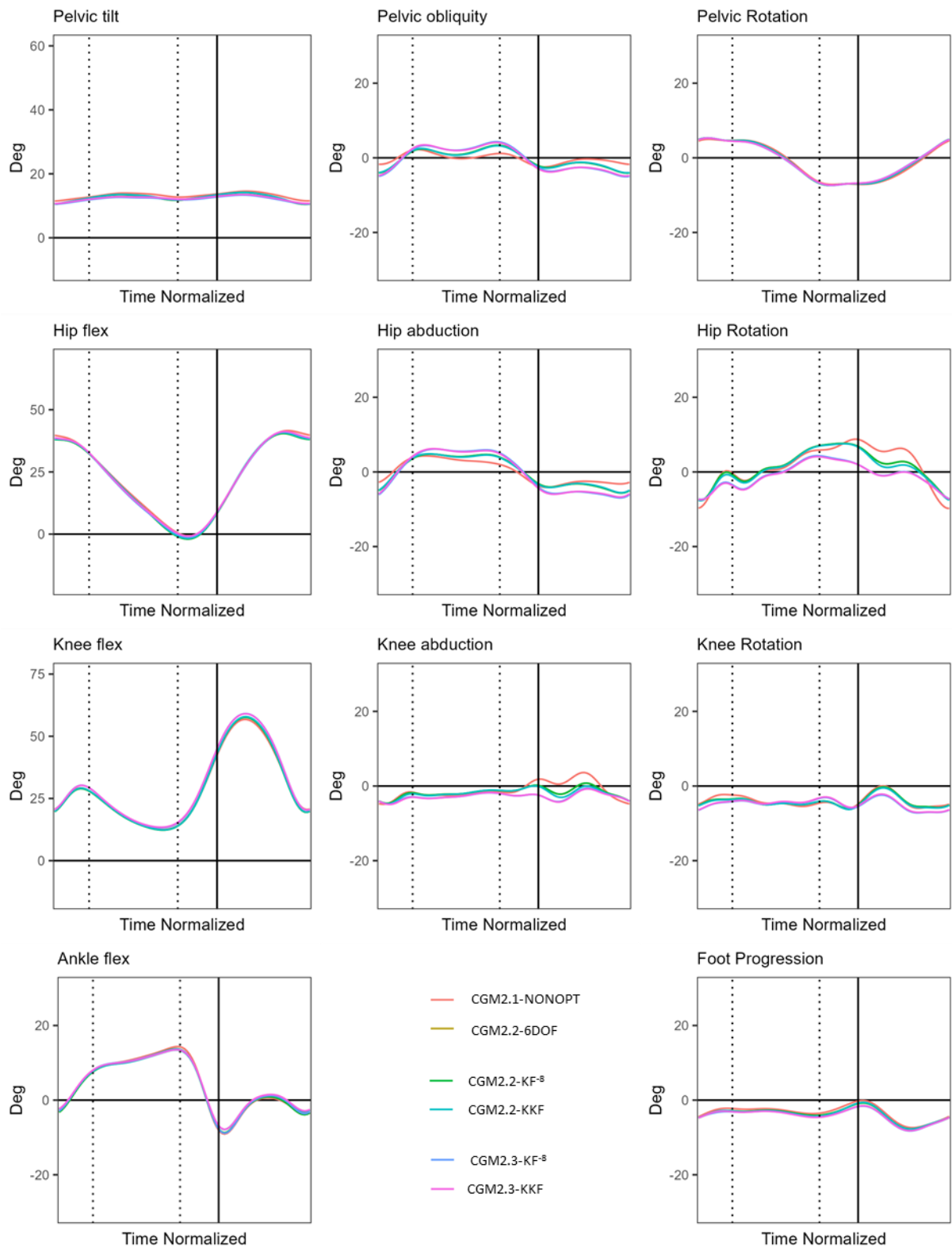


Table 1

Cliquez ou appuyez ici pour entrer du texte.

Label	Description	Marker type
(L/R)ASI	Antero-superior iliac spine	Anatomical and Technical
(L/R)PSI	Postero-superior iliac spine	Anatomical and Technical
(L/R)THI	Thigh wand marker. Place below the THL marker	Technical
(L/R)THAP	on front of thigh in midline and about $\frac{1}{4}$ the distance from hip to knee	Technical
(L/R)THAD	on front of thigh in midline and about and $\frac{3}{4}$ the distance from hip to knee	Technical
(L/R)KNE	Lateral epicondyle of the femur	Anatomical and Technical
(L/R)KNM	Medial epicondyle of the femur	Anatomical
(L/R)TIB	Shank wand marker. Place below the THL marker	Technical
(L/R)TIAP	2cm distal to the most prominent aspect of the tibial tubercle	Technical
(L/R)TIAD	on the tibial crest in midline and about and $\frac{3}{4}$ the distance from knee to ankle	Technical
(L/R)ANK	Lateral malleolus	Anatomical and Technical
(L/R)MED	Medial malleolus	Anatomical
(L/R)HEE	Posterior calcaneus	Anatomical and Technical
(L/R)TOE	Metatarso-cuneiform joint	Anatomical and Technical

Cliquez ou appuyez ici pour entrer du texte.

Table 2

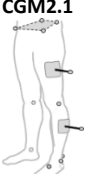
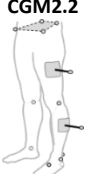

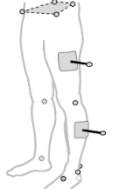
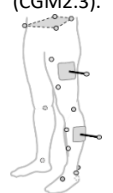
								
		6DOF largest diff: Avg (sd)-max	KF⁵ largest diff: Avg (sd)-max	KF⁸ largest diff: Avg (sd)-max	KKF largest diff: Avg (sd)-max	KF⁵ largest diff: Avg (sd)- max	KF⁸ largest diff: Avg (sd)-max	KKF largest diff: Avg (sd)-max
CGM2.1-NON-OPT comparisons	TD	Hip rotation: 2.1(0.6)- 3.9	Hip rotation: 2.1(0.6)- 3.9	Hip rotation: 2.1(0.6)- 3.9	Hip rotation: 2.2(0.6)- 3.7	Hip rotation: 3.8(0.7)-4.6	Hip rotation: 3.8(0.7)-4.6	Hip rotation: 3.8(0.7)-4.6
	CP	Hip rotation: 2.6(0.8)- 4.2	Hip rotation: 2.6(0.1)- 4.2	Hip rotation: 2.6(0.1)- 4.2	Hip rotation: 2.0(0.1)- 4.3	Hip rotation: 4.1(1.0)-5.9	Hip rotation: 4.1(1.0)-5.9	Hip rotation: 4.1(1.0)-5.8
within- markerset – between KF methods	CGM2.2 KF⁵	TD		MADs<1°	MADs<1°			
		CP						
	CGM2.2 KF⁸	TD					MADs<1°	
		CP						
	CGM2.3 KF⁵	TD					MADs<1°	MADs<1°
		CP						
between- markersets – within KF method	CGM2.2 KF⁵	TD				Hip rotation: 3.3(1.0)-6.5		
		CP				Hip rotation: 3.2(1.8)-7.7		
	CGM2.2 KF⁸	TD					Hip rotation: 3.7(1.0)-6.7	
		CP					Hip rotation: 3.3(1.7)-6.9	
	CGM2.2 KKF	TD						Hip rotation: 3.2(1.0)-6.0
		CP						Hip rotation: 3.3(1.7)-6.9

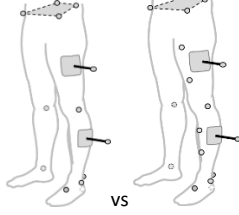
Table 3

	Parameters		R ² 6DOF vs NONOPT Avg(sd)		R ² KF ⁸ vs NONOPT Avg(sd)		R ² KF ⁵ vs NONOPT Avg(sd)		R ² KKF vs NONOPT Avg(sd)		R ² KF ⁸ vs KKF Avg(sd)		R ² KF ⁵ vs KKF Avg(sd)		R ² KF ⁵ vs KF ⁸ Avg(sd)	
			TD	CP	TD	CP	TD	CP	TD	CP	TD	CP	TD	CP		
Native markerset (CGM2.1- CGM2.2). 	Pelvis	Tilt	0.8	0.9	0.8	0.9	0.8	0.9	0.8	0.9	>0.95					
		Obl	0.7	0.7	0.7	0.7	0.7	0.7	0.7	0.7						
		Rot	1.0	1.0	1.0	1.0	1.0	1.0	1.0	1.0						
	Hip	Fle	1.0	1.0	1.0	1.0	1.0	1.0	1.0	1.0						
		Abd	0.9	0.9	0.9	0.9	0.9	0.9	0.9	0.9						
		Rot	0.9	0.9	0.9	0.9	0.9	0.9	0.8	0.8						
	knee	Fle	1.0	1.0	1.0	1.0	1.0	1.0	1.0	1.0						
		Abd	0.7	0.9	0.7	0.9	0.7	0.9	0.6	0.8						
		Rot	0.9	1.0	0.9	1.0	0.9	1.0	0.9	1.0						
	Anklep	Fle	1.0	1.0	1.0	1.0	1.0	1.0	1.0	1.0						
footProgression			1.0	1.0	1.0	1.0	1.0	1.0	1.0							

Cliquez ou appuyez ici pour entrer du texte.

	Pelvis	Tilt			0.8	0.9	0.8	0.9	0.8	0.9	>0.95
		Obl			0.6	0.6	0.6	0.6	0.6	0.7	
		Rot			1.0	1.0	1.0	1.0	1.0	1.0	
	Hip	Fle			1.0	1.0	1.0	1.0	1.0	1.0	
		Abd			0.9	0.8	0.9	0.8	0.9	0.8	
		Rot			0.5	0.7	0.5	0.7	0.5	0.7	
	Knee	Fle			1.0	1.0	1.0	1.0	1.0	1.0	
		Abd			0.5	0.7	0.5	0.7	0.5	0.7	
		Rot			0.7	0.8	0.7	0.8	0.7	0.8	
	Ankle	Fle			1.0	1.0	1.0	1.0	1.0	1.0	
	FootProgression				1.0	1.0	1.0	1.0	1.0	1.0	

a)

	Parameters		R ² KF ⁻⁸		R ² KF ⁻⁵		R ² KKF	
			Avg(sd)		Avg(sd)		Avg(sd)	
	Pelvis	Tilt	0.8	0.9	0.8	0.9	0.8	0.9
		Obl	0.9	0.9	0.9	0.9	0.9	0.9
		Rot	1.0	1.0	1.0	1.0	1.0	1.0
	Hip	Fle	1.0	1.0	1.0	1.0	1.0	1.0
		Abd	1.0	1.0	1.0	1.0	1.0	1.0
		Rot	0.7	0.8	0.7	0.8	0.7	0.8
	Knee	Fle	1.0	1.0	1.0	1.0	1.0	1.0
		Abd	0.8	0.8	0.8	0.8	0.8	0.9
		Rot	0.7	0.8	0.7	0.8	0.7	0.9
	Ankle	Fle	1.0	1.0	1.0	1.0	1.0	1.0
	FootProgression		1.0	1.0	1.0	1.0	1.0	1.0

b)